

GENERAL ARTICLE

The number of the CTCF binding sites of the *H19/IGF2:IG-DMR* correlates with DNA methylation and expression imprinting in a humanized mouse model

Andrea Freschi^{1,2,†}, Rosita Del Prete^{1,†}, Laura Pignata¹, Francesco Cecere^{1,3}, Francesco Manfredola⁴, Monica Mattia⁴, Gilda Cobellis⁴, Angela Sparago¹, Marisa S. Bartolomei⁵, Andrea Riccio^{1,3,*} and Flavia Cerrato^{1,*}

¹Department of Environmental Biological and Pharmaceutical Sciences and Technologies (DiSTABiF), Università degli Studi della Campania “Luigi Vanvitelli”, Caserta 81100, Italy, ²Genetics and Epigenetics of Behaviour (GEB), Istituto Italiano di Tecnologia (IIT), Genova 16163, Italy, ³Institute of Genetics and Biophysics (IGB) “Adriano Buzzati-Traverso”, Consiglio Nazionale delle Ricerche (CNR), Naples 80131, Italy, ⁴Department of Experimental Medicine, Università degli Studi della Campania “Luigi Vanvitelli”, Naples 80138, Italy and ⁵Department of Cell and Developmental Biology, Epigenetics Institute, Perelman School of Medicine at the University of Pennsylvania, Philadelphia, PA 19104, USA

*To whom correspondence should be addressed. Tel: +39 0823 274415; Fax: +39 0823 274605; Email: flavia.cerrato@unicampania.it (Flavia Cerrato); Tel: +390 816 132 444; Email: andrea.riccio@unicampania.it (Andrea Riccio)

Abstract

The reciprocal parent of origin-specific expression of *H19* and *IGF2* is controlled by the *H19/IGF2:IG-DMR* (IC1), whose maternal allele is unmethylated and acts as a CTCF-dependent insulator. In humans, internal IC1 deletions are associated with Beckwith–Wiedemann syndrome (BWS) and Silver-Russell syndrome (SRS), depending on their parental origin. These genetic mutations result in aberrant DNA methylation, deregulation of *IGF2/H19* and disease with incomplete penetrance. However, the mechanism linking the microdeletions to altered molecular and clinical phenotypes remains unclear. To address this issue, we have previously generated and characterized two knock-in mouse lines with the human wild-type (hIC1wt) or mutant (hIC1Δ2.2) IC1 allele replacing the endogenous mouse IC1 (mIC1). Here, we report an additional knock-in line carrying a mutant hIC1 allele with an internal 1.8 kb deletion (hIC1Δ1.8). The phenotype of these mice is different from that of the hIC1Δ2.2-carrying mice, partially resembling hIC1wt animals. Indeed, proper *H19* and *Igf2* imprinting and normal growth phenotype were evident in the mice with maternal transmission of hIC1Δ1.8, while low DNA methylation and non-viable phenotype characterize its paternal transmission. In contrast to hIC1wt, E15.5 embryos that paternally inherit hIC1Δ1.8 displayed variegated hIC1 methylation. In addition, increased *Igf2* expression, correlating with increased body weight, was found in one third of these mice. Chromatin immunoprecipitation experiments in mouse embryonic stem cells

[†]These authors contributed equally.

Received: March 1, 2021. Revised: April 23, 2021. Accepted: April 26, 2021

© The Author(s) 2021. Published by Oxford University Press.

This is an Open Access article distributed under the terms of the Creative Commons Attribution Non-Commercial License (<http://creativecommons.org/licenses/by-nc/4.0/>), which permits non-commercial re-use, distribution, and reproduction in any medium, provided the original work is properly cited. For commercial re-use, please contact journals.permissions@oup.com

carrying the three different hIC1 alleles demonstrate that the number of CTCF target sites influences its binding to hIC1, indicating that in the mouse, CTCF binding is key to determining hIC1 methylation and *Igf2* expression.

Introduction

Genomic imprinting is an epigenetic process causing monoallelic and parent-of-origin-dependent expression of a small subset of mammalian genes. Imprinted genes play a key role in the development of mammals, and most of them are organized in clusters. Usually, an Imprinting Control Region (ICR or IC) regulates the differential expression of the genes of the cluster. ICs are 2–5 kb-long genomic sequences displaying differential DNA methylation between their maternal and paternal alleles. IC methylation is established during gametogenesis, and maintained throughout development, despite extensive demethylation occurring in the embryonic genome before implantation, and *de novo* methylation occurring after implantation (1). Proper methylation of the ICs is required for correct imprinting of the gene cluster. A number of oocyte and zygotic factors are involved in the processes of *de novo* methylation and maintenance of differential methylation of the ICs in the gametes and early embryo (2). In humans, aberrant IC methylation as well as uniparental disomy, genetic mutations and copy number variants affecting imprinted loci are associated with several diseases characterized by disturbances of growth, metabolism and behavior that are globally classified as Imprinting Disorders.

The imprinted domain harboring the *H19* and *Insulin-like growth factor 2 (Igf2)* genes maps to the mouse distal chromosome 7 and is orthologous with the telomeric domain of the human chromosome 11p15.5 cluster (3). The *Igf2* gene is expressed from the paternal allele and encodes a protein promoting fetal growth (4). The *H19* gene is expressed from the maternal allele and encodes a long non-coding RNA with growth inhibitory properties (5). The *H19* RNA also releases miR-675 late in gestation to suppress the growth of the placenta just before birth (6). The reciprocal imprinting of *Igf2* and *H19* is regulated by an ICR (also known as *H19/IGF2:IG-DMR* or IC1 in humans) that is methylated on the paternal chromosome. The unmethylated maternal IC1 allele interacts with the CCCTC-binding factor (CCTF), thus generating an insulator that through long-range chromosome interactions interferes with the access of the *Igf2* promoter to enhancers that are located downstream of *H19* (7). Methylation of the paternal IC1 inhibits CTCF binding and insulator function, allowing interaction of the enhancers with the *Igf2* but not with the *H19* promoter, which instead acquires DNA methylation during development. This results in transcriptional activation of *H19* and silencing of *Igf2* on the maternal chromosome, and *Igf2* activation and *H19* silencing on the paternal chromosome (8,9).

In humans, deregulation of the *H19* and *IGF2* genes is associated with two imprinting disorders, Beckwith–Wiedemann syndrome (BWS, MIM #130650) and Silver–Russell syndrome (SRS, MIM #180860), which are characterized by somatic overgrowth and undergrowth, respectively. Opposite DNA methylation defects can be found at IC1 in BWS and SRS patients. Gain of methylation (GOM) of the maternal allele and loss of methylation (LOM) of the paternal allele cause reciprocal changes of *H19* and *IGF2* expression in BWS and SRS, respectively (10,11). Also, IC1 GOM represents the molecular defect of BWS with the highest risk of developing Wilms tumors (12). Although most of the cases with IC1 methylation defects are sporadic, rare familial cases in which internal IC1 deletions are associated with aberrant DNA methylation and *H19/IGF2* deregulation have

been described (13–19). It has been proposed that these deletions alter the binding of proteins preventing DNA methylation, such as CTCF, on the maternal allele, and the binding of proteins maintaining DNA methylation, such as ZFP57, on the paternal allele (15). Nevertheless, the mechanism linking these genetic defects with the altered molecular and clinical phenotypes has not yet been demonstrated.

Although the function of IC1 appears well conserved, its DNA sequence is very different in the human and mouse species. While the human IC1 (hIC1) contains seven CTCF target sites (CTSs) included in repetitive sequences overall spanning about 5 kb, the mouse IC1 (mIC1) is shorter (about 2 kb), non-repetitive and contains only four CTSs (3) (Fig. 1A). Also, the number of the ZFP57 target sites (ZTSs) differs between hIC1 and mIC1, with the former harboring 12 ZTSs and the latter only six (Fig. 1A).

To clarify the role of hIC1 mutations in the origin of imprinting defects, we have previously generated and characterized two knock-in (KI) mouse lines in which the murine IC1 (mIC1) is replaced by the orthologous human sequence in either wild-type (hIC1wt) or mutant (hIC1 Δ 2.2) form. In the latter case, the IC1 allele carrying a 2.2 kb deletion found in a BWS family was chosen (17). The mice carrying the hIC1wt allele showed normal IC1 methylation, *H19* and *Igf2* expression and growth phenotype on maternal transmission, but disrupted imprinting, severe growth restriction and a non-viable phenotype on paternal transmission (20). Conversely, the mice carrying the hIC1 Δ 2.2 allele were viable, but with tissue-specific and mosaic imprinting alterations and pre/post-natal overgrowth on maternal transmission and undergrowth on paternal transmission. To further investigate the mechanism causing such unexpected behavior of the human IC1 alleles in the mouse context, we have now generated and characterized an additional humanized mouse line carrying an hIC1 allele with an internal 1.8 kb deletion, which was found in another familial BWS case (13). The comparison of this line with the previous lines indicates that in the mouse context the number of CTSs of hIC1 is crucial for the maintenance of imprinting at the *Igf2/H19* locus.

Results

Generation of the hIC1 Δ 1.8 line

To better understand the molecular mechanisms linking epimutations and clinical phenotype with hIC1 sequence, we extended our previous studies by generating a new humanized mouse line, in which the endogenous mIC1 was replaced with a mutant hIC1 allele carrying the deletion of 1.8 kb that was previously found in a familial BWS case (13) (Fig. 1; see also Materials and Methods). Once the germ line transmission of the KI was established, we crossed heterozygous KI (having C57BL/6 background) with wild-type Balb/C mice and typed polymorphic sites in the F1 hybrid progeny to distinguish the parental origin of the *H19* and *Igf2* alleles in all molecular analyses. Wild-type littermates were used as control animals.

Maternal transmission of the hIC1 Δ 1.8 allele does not affect growth and *H19/Igf2* imprinting.

To determine the effect of the hIC1 Δ 1.8 allele on somatic growth, we measured the weight of the progeny of $H19^{hIC1\Delta 1.8/+} \times H19^{+/+}$ mice (conventionally, the order of the alleles of the

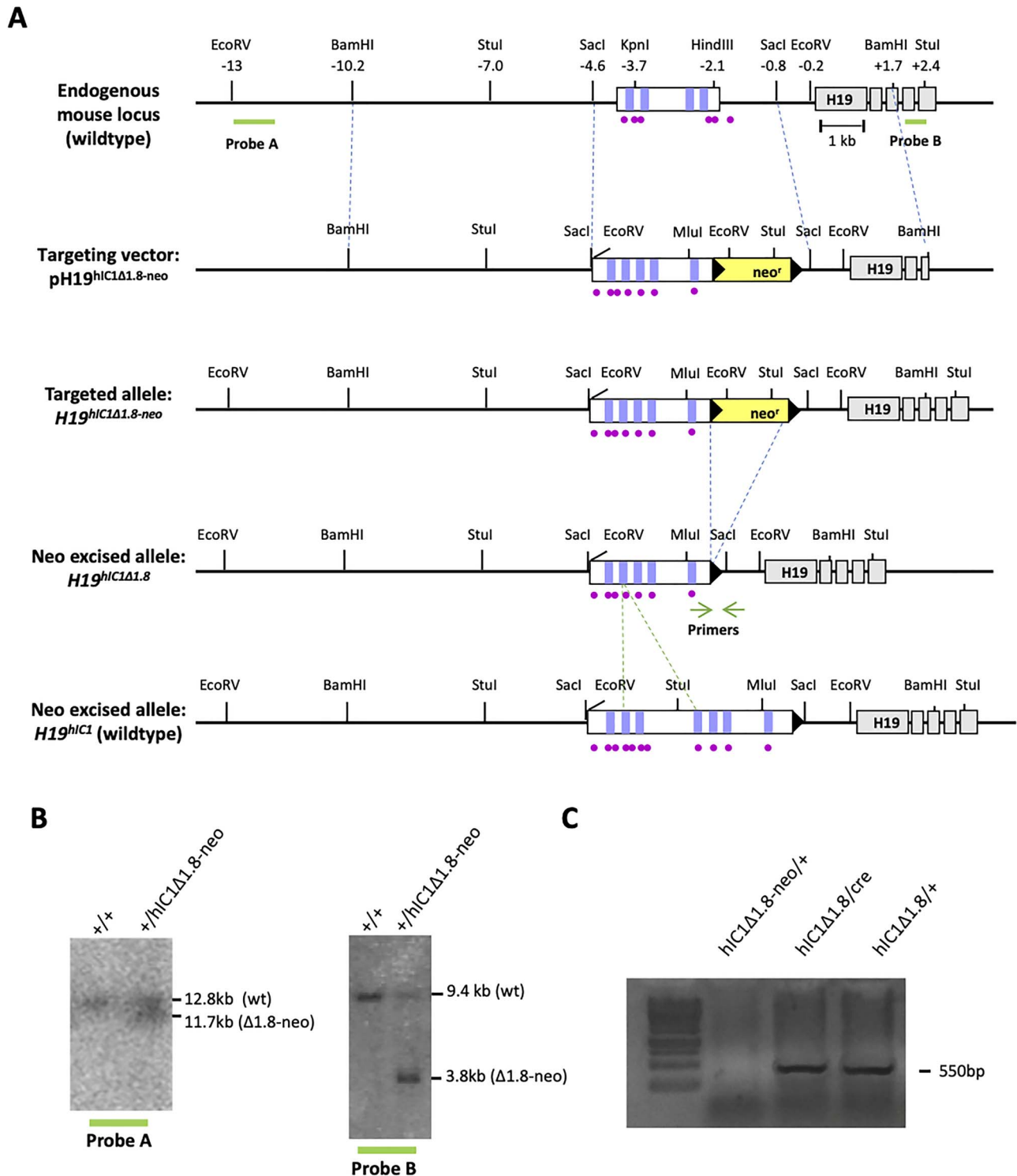


Figure 1. Generation of the $hIC1^{\Delta 1.8}$ allele. (A) From the top: the mouse *H19* endogenous locus, the targeting vector ($pH19^{hIC1\Delta 1.8-neo}$), the correctly targeted allele with the neomycin resistance cassette ($H19^{hIC1\Delta 1.8-neo}$), the targeted allele after neoR excision ($H19^{hIC1\Delta 1.8}$) and the targeted wild-type human allele ($H19^{hIC1}$). The white rectangle depicts IC1 with the CTCF binding sites (vertical lilac bars) and ZFP57 target sites (purple circles), *H19* exons (gray rectangles), neoR cassette (yellow rectangle), loxP sites (black arrowheads); pBluescriptIIKS vector with the human insert flanked by the mouse sequences (outlined with dashed blue lines) used as arms for the homologous recombination. Restriction sites and their relative positions (in kb) to the *H19* transcription start site are also indicated. The probes (A and B) used for Southern blot screening are indicated as green lines below the endogenous locus and the PCR primers used for confirming neoR excision are indicated with green arrows. (B) Southern blot analysis confirming the targeting of the mutant IC1 allele was carried out on EcoRV digested wild-type (+/+) and targeted (+/ $hIC1^{\Delta 1.8-neo}$) ES cell DNA hybridized to the probe A (lying 5' of the targeting arm) or on StuI digested DNA hybridized to the probe B (lying 3' of the targeting arm). (C) Correctly Cre-mediated excision of neoR was confirmed by a PCR product of 550 bp from F1 mice ($hIC1^{\Delta 1.8}/cre$) and F2 ($hIC1^{\Delta 1.8}/+$), while no amplification was assessed for mice with the neoR cassette.

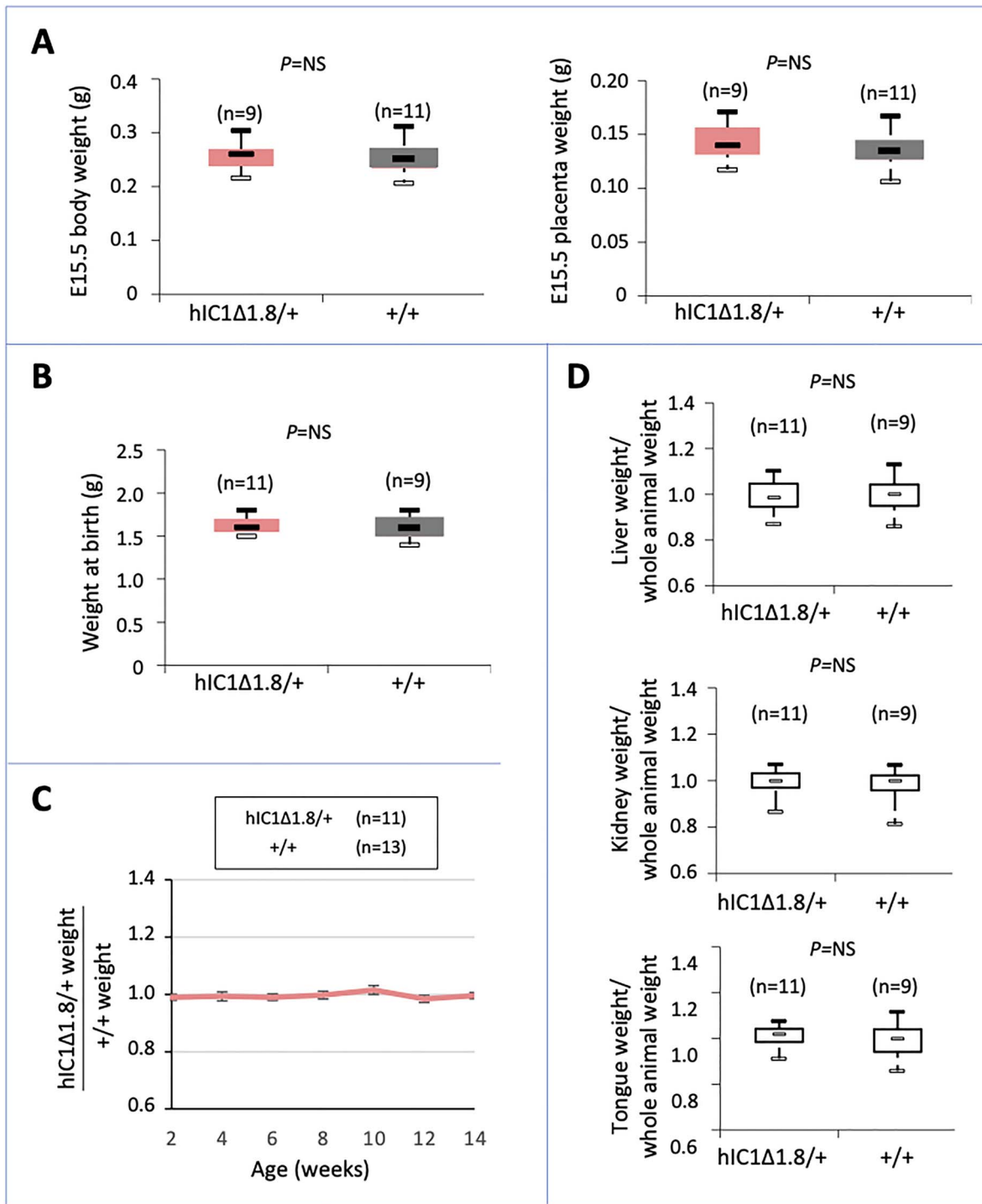


Figure 2. Normal somatic growth on maternal transmission of the $hIC1^{\Delta 1.8}$ allele. Box plots of weights of (A) E15.5 embryo body and placenta and (B) newborn (P1) mice, (C) growth chart and (D) box plots of organ/whole animal weights of mice at 14 weeks of age. Box plots display the full range of variation (from minimum to maximum value), the likely range of variation (the first and third quartiles), and the median (the horizontal bar within box). Values in brackets indicate the number of animals derived from three litters of 6–8 pups each, and analyzed in the present study. P = P -value calculated by two-tailed Student's T -test. In (C) the growth chart represents the ratio between weights of $H19^{hIC1\Delta 1.8/+}$ and $H19^{+/+}$ mice of three litters. Bars represent the mean \pm SEM. In (D) the box plots represent the relative values of organ weight/whole animal weight ratios, obtained by arbitrarily setting the median value of $H19^{+/+}$ as 1.

genotype is: maternal/paternal) at different developmental stages (Fig. 2). Comparable weights of body and placenta were found in KI mice and their wild-type littermates at embryonic day 15.5 (E15.5, Fig. 2A), birth (P1, Fig. 2B) and postnatally until 14 weeks of age (Fig. 2C). Also, the weights of kidney, liver

and tongue of adult KI and wild-type mice did not show any statistically significant difference (Fig. 2D).

Gene expression and DNA methylation of the $H19/Igf2$ locus were analyzed in the body and placenta of E15.5 embryos, as well as liver, kidney and tongue of P1 mice. We found that the

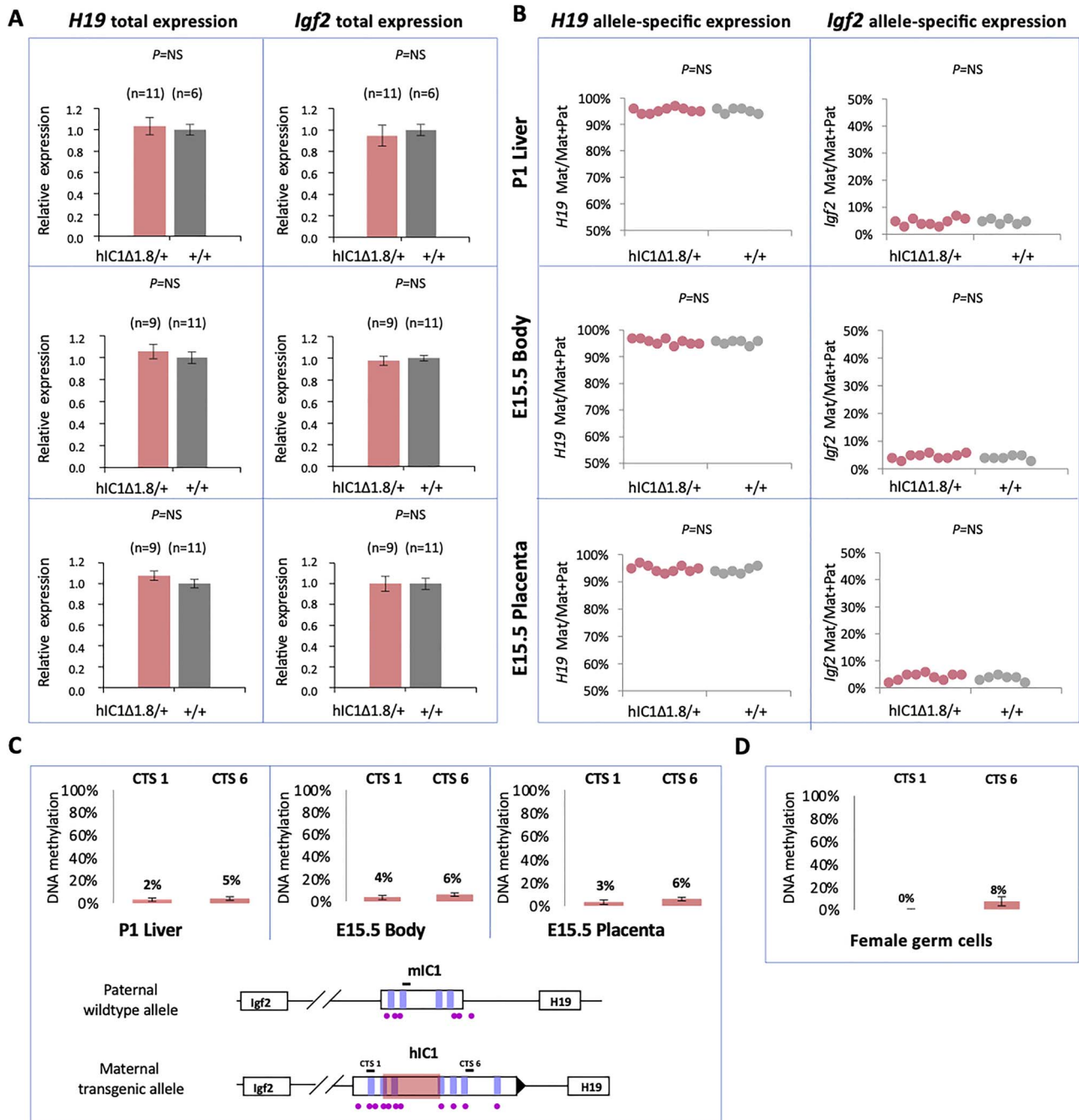


Figure 3. Expression and DNA methylation analysis in *H19*^{hIC1Δ1.8/+} mice. (A) Histograms of total *H19* and *Igf2* expression in neonatal liver, embryo body and placenta at E15.5 of *H19*^{hIC1Δ1.8/+} and *H19*^{+/+} littermates analyzed by RT-qPCR. (B) Allele-specific expression of *H19* and *Igf2*. Dots indicate the percent expression of the maternal allele in each sample. (C) Graphs of DNA methylation analysis at IC1 in *H19*^{hIC1Δ1.8/+} mice. Percent of DNA methylation measured by pyrosequencing at two CTCF target sites (CTS1 and CTS6) in P1 liver, E15.5 embryo body and placenta, collected from *H19*^{hIC1Δ1.8/+} mice. Each histogram represents the mean value of the methylation level of 5 (CTS 1) or 6 (CTS 6) CpGs, tested in *H19*^{hIC1Δ1.8/+} (n = 11/9) and *H19*^{+/+} (n = 6/11) mice. On the bottom, schematic representation of the humanized and the endogenous IC1: the black bars indicate the analyzed region (see Supplementary Material, Figure S2 for the endogenous control values). A shaded pink box indicates the deleted region of *H19*^{hIC1Δ1.8}. For other details, see legend to Figure 1A. (D) Percent methylation measured by pyrosequencing at CTS1 and CTS6 in a pool of oocytes collected from four *H19*^{hIC1Δ1.8/+} females. Values in brackets indicate the number of analyzed animals in these experiments; they derived from three litters of 6–8 pups each. NS, Not Significant. Bars represent the mean ± SEM.

H19^{hIC1Δ1.8/+} mice had total (Fig. 3A and Supplementary Material, Fig. S1A) and allele-specific (Fig. 3B and Supplementary Material, Fig. S1B) expression of *H19* and *Igf2* similar to their *H19*^{+/+} littermates in all the analyzed tissues. DNA methylation of two CTCF target sites, CTS1 and CTS6, found exclusively in the human

sequences on the maternal chromosome, was tested by pyrosequencing of bisulfite-converted DNA. Similar to the endogenous maternal mIC1, very low methylation levels (1–6%) were detected in both E15.5 and P1 tissues (Fig. 3C, Supplementary Material, Figs S1C and S2A). Low methylation was detected also at CTS1

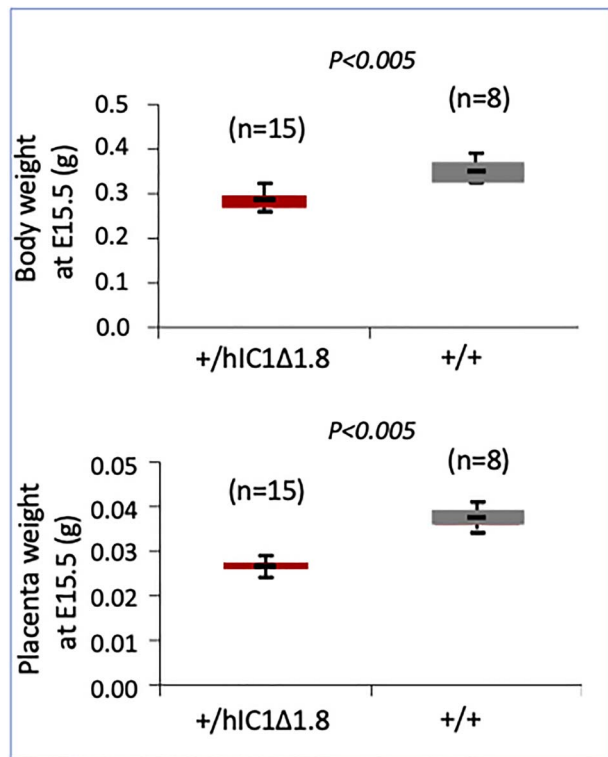


Figure 4. Growth restriction on paternal transmission of the *h1C1*^{Δ1.8} allele. Box plots of embryo body and placenta weights at E15.5. The analyzed animals derived from three litters of 6–8 pups each. See also legend to [Figure 2](#).

and CTS6 (0 and 8%, respectively) in oocytes of the *H19*^{+/+}*h1C1*^{Δ1.8/+} females ([Fig. 3D](#) and [Supplementary Material, Fig. S2B](#)).

Paternal transmission of the *h1C1*^{Δ1.8} allele is embryonic lethal and results in *Igf2* down-regulation and loss of *H19* imprinting

We then investigated the effect of paternal transmission of the *h1C1*^{Δ1.8} allele. We observed that in 10 litters derived from *H19*^{+/+} × *H19*^{h1C1}^{Δ1.8/+} breedings, the number of live pups/litter was reduced to about 50% that of maternal transmission, and only wild-type live-born mice were found, suggesting that paternal transmission of the *h1C1*^{Δ1.8} allele was embryonic lethal. Consistent with this hypothesis, we found that when analyzed at E15.5, viable *H19*^{+/+}*h1C1*^{Δ1.8} and *H19*^{+/+} embryos were observed in similar proportion. A severe growth deficiency of the *H19*^{+/+}*h1C1*^{Δ1.8} conceptuses, however, was noted in these mice. The weight of their body and placenta was significantly lower (~25 and ~30%, respectively) than those of *H19*^{+/+} littermates ([Fig. 4](#)).

Total and allele-specific gene expression of the *H19* and *Igf2* genes were performed on body and placenta of the *H19*^{+/+}*h1C1*^{Δ1.8} and *H19*^{+/+} conceptuses at E15.5. Total *H19* expression was increased in body and placenta of the *H19*^{+/+}*h1C1*^{Δ1.8} embryos ([Fig. 5A](#)). Conversely, *Igf2* expression was strongly decreased in both body and placenta of the *H19*^{+/+}*h1C1*^{Δ1.8} line ([Fig. 5A](#)). Analysis of allele-specific expression demonstrated comparable levels of the maternal and paternal *H19* alleles in these tissues (40–50% pat/mat + pat), indicating complete loss of *H19* imprinting, in *H19*^{+/+}*h1C1*^{Δ1.8} conceptuses ([Fig. 5B](#)). In contrast, *Igf2* imprinting was normal and only its paternal allele was expressed, although at a lower level.

h1C1 methylation was then analyzed in the *H19*^{+/+}*h1C1*^{Δ1.8} conceptuses by pyrosequencing. Methylation levels of *h1C1* detected in body (CTS1=10%, CTS6=8%) and placenta (CTS1=14%, CTS6=13%) of the analyzed embryos were on average much lower than that of the endogenous paternal *m1C1* (100%) ([Fig. 5C](#) and [Supplementary Material, Fig. S2A](#)). When sperm of adult *H19*^{h1C1}^{Δ1.8/+} mice was investigated, methylation levels were lower at *h1C1* (CTS1=45%, CTS6=38%; [Fig. 5D](#), top) than at the endogenous *m1C1*, which was fully methylated ([Supplementary Material, Fig. S2B](#), lower panel). Incomplete *h1C1* methylation in sperm of these mice was confirmed by bisulfite treatment followed by cloning and sequencing ([Fig. 5D](#), bottom). These results indicate that DNA methylation of the *h1C1*^{Δ1.8} allele is properly established only in about one third of the male germ cells during spermatogenesis.

Variegated *h1C1* methylation and *Igf2* expression in *H19*^{+/+}*h1C1*^{Δ1.8} embryos

Although the average *h1C1* methylation was very low in *H19*^{+/+}*h1C1*^{Δ1.8} embryos, we observed a strong heterogeneity among individual animals ([Fig. 6A and B](#)). Within the 15 individuals analyzed, 10 showed levels <5%, while five (#4, #5, #9, #10, #11) had relatively higher methylation levels in both body (20–35%) and placenta (20–40%). Interestingly, increased *Igf2* but similar *H19* expression was found in the samples (#4, #5, #9, #10, #11) with higher methylation values, particularly in placenta ([Fig. 6C and D](#)). Also, CTS1/CT6 methylation and *Igf2*—but not *H19*—expression were directly correlated with body weight in E15.5 embryos ([Fig. 6E](#) and [Supplementary Material, Fig. S3](#)).

Differential CTCF binding at *h1C1* alleles in mouse ES cells

To get further insights into the mechanism of DNA methylation maintenance at *h1C1*, we analyzed the binding of CTCF and ZFP57 to the *h1C1*^{Δ1.8} allele by chromatin immunoprecipitation in mouse ES cells (ESCs), and compared it with the binding of these proteins to *h1C1*wt and *h1C1*^{Δ2.2}. The amount of a DNA fragment (CTS1) that is unaffected by the deletions was measured by quantitative real-time PCR in the immunoprecipitated DNA. We found that CTCF was about 50% less enriched on CTS1 in the ESCs carrying the *h1C1*^{Δ2.2} allele compared to the ESCs carrying the *h1C1*^{Δ1.8} or the *h1C1*wt alleles ([Fig. 7A](#)). Conversely, no difference was observed in CTCF binding at the endogenous *m1C1*, *Plagl1* and *Gapdh* loci, nor in ZFP57 and H3K4me3 enrichment at these loci, in the three ESC lines carrying the different *h1C1* alleles. Comparable levels (20–25%) of CTS1 methylation was demonstrated in the three ESC lines, thus excluding that the difference in CTCF binding was caused by differential DNA methylation acquired during cell culture ([Fig. 7B](#)).

Discussion

In BWS and SRS, *IC1* imprinting defects may arise as primary epigenetic mutation or as consequence of an internal deletion. The latter mechanism is less frequent, but is characterized by higher recurrence risk (14,21). We have previously suggested that the penetrance and expressivity of the clinical phenotype associated with internal *IC1* deletions are influenced by their parental origin, as well as by the transcription factor binding sites and their arrangement affected by the mutation (15). However, the molecular mechanisms underlying *h1C1* hyper-

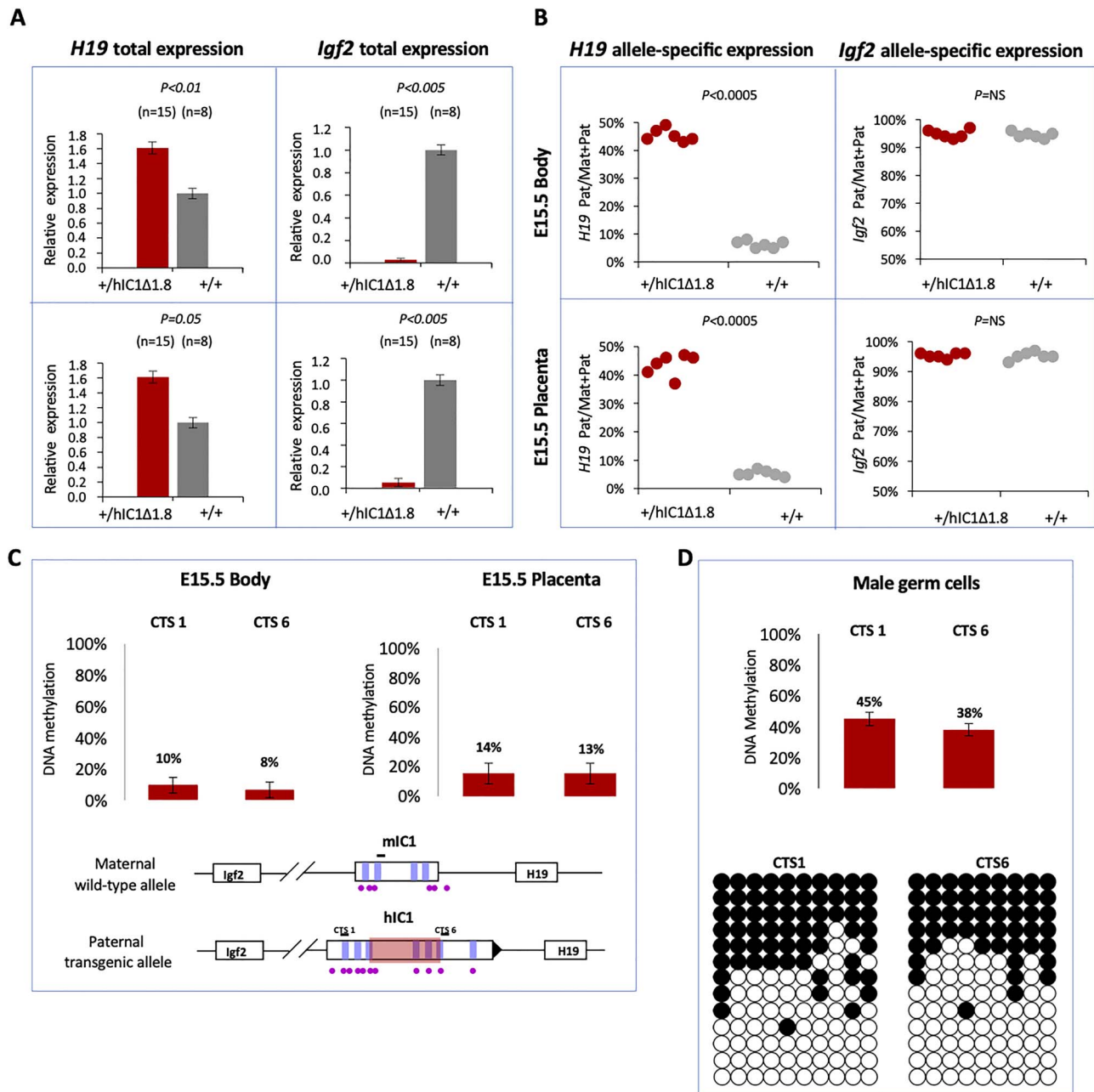


Figure 5. Expression and DNA methylation analysis in $H19^{+/h1c1\Delta1.8}$ mice at E15.5. (A) Histograms of total $H19$ and $Igf2$ expression in E15.5 embryo body and placenta of $H19^{+/h1c1\Delta1.8}$ and $H19^{+/+}$ littermates analyzed by RT-qPCR. (B) Allele-specific expression of $H19$ and $Igf2$. Dots indicate the percent expression of the paternal allele in each individual sample. (C) DNA methylation analysis at CTS1 and CTS6 of embryo body and placenta collected from $H19^{+/h1c1\Delta1.8}$ conceptuses. See also legend to Figure 3. (D) Top: percent methylation measured by pyrosequencing at CTS1 and CTS6 in a pool of male germ cells collected from two $H19^{h1c1\Delta1.8/+}$ males. Bottom: the same regions were also analyzed by bisulphite treatment followed by cloning and sequencing. Each line corresponds to a single template DNA molecule cloned; each circle corresponds to a CpG dinucleotide. Filled circles designate methylated cytosines; open circles, unmethylated cytosines.

and hypo-methylation remain undemonstrated and the relationship between IC1 mutations and epimutations and clinical phenotypes still far from being completely understood (11,22). To increase our understanding of this issue, we have generated a number of humanized mouse lines, in which the orthologous human wild-type or mutant IC1 sequence replaced the endogenous locus. In the present study, we report the characterization of a second mutant line, hIC1 Δ 1.8, which carries a smaller hIC1 deletion and lacks two CTSs instead of three, with respect to the previously described hIC1 Δ 2.2 (Fig. 8A). Overall, the phenotype

of the hIC1 Δ 1.8 mice was found intermediate between that of the hIC1wt and hIC1 Δ 2.2 lines, suggesting that in the mouse context the number of CTCF binding sites has a crucial role in maintenance of hIC1 methylation and $H19/Igf2$ expression.

On maternal transmission, the phenotype of the hIC1 Δ 1.8 mice is similar to that of hIC1wt. Both the hIC1 Δ 1.8 and hIC1wt lines showed proper $H19/Igf2$ imprinting and normal pre/postnatal growth (20). Conversely, the hIC1 Δ 2.2 line showed partial gain of methylation, increased $Igf2$ and decreased $H19$ expression and pre- and post-natal overgrowth. (Fig. 8B) (23). On paternal

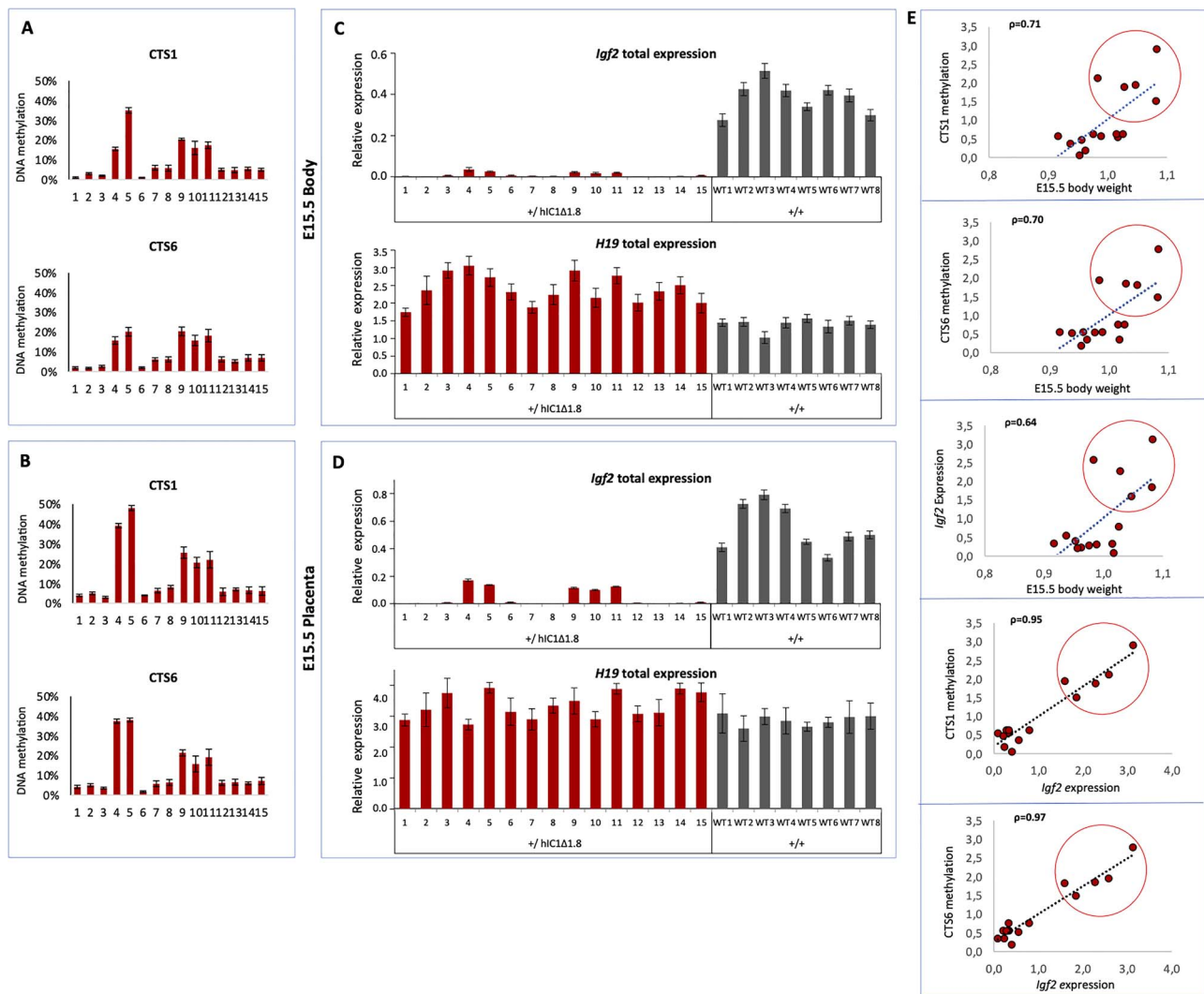


Figure 6. DNA methylation and expression analysis at the *H19/Igf2* locus in individual samples of *H19*^{+/h1C1Δ1.8} mice at E15.5. (A and B) DNA methylation of CTS1 and CTS6 and (C and D) *Igf2* and *H19* expression levels in individual embryos. Bars represent the mean \pm SEM of three technical replicates of the same sample. (E) Plots of the Pearson's linear correlation coefficients between all pairs of the following parameters: body weights, methylation of CTS1 and CTS6, total expression of *Igf2*. Each dot represents the values of each mouse relative to the mean of its own litter. The red circle includes the animals with higher methylation values (#4, #5, #9, #10, #11). The trend line and the ρ coefficient of Pearson correlation are shown in each plot.

transmission, both h1C1Δ1.8 and h1C1wt mice are characterized by IC1 hypomethylation and severe growth restriction, and are not viable (Fig. 8B). However, the imprinting defect of h1C1Δ1.8 is less dramatic than that of h1C1wt. In one third of the animals inheriting the h1C1Δ1.8 allele from their father, IC1 methylation was relatively higher and *Igf2* expression not completely silenced as in the h1C1wt line. Consistent with this finding, growth restriction was less severe in the pat h1C1Δ1.8 than in the pat h1C1wt mice, although probably not enough to be compatible with post-natal life. As proposed for the h1C1wt line (20), it is likely that increased *H19* coupled with lower *Igf2* expression is responsible for the lethal phenotype of the *H19*^{+/h1C1Δ1.8} mice. In contrast to h1C1Δ1.8 and h1C1wt, paternal transmission of the h1C1Δ2.2 allele is associated with partial IC1 methylation, decreased *Igf2*, increased *H19* and pre/post-natal growth restriction (Fig. 8B) (23).

The analysis of the gametes and embryos indicates that all the three humanized IC1 lines fail to properly acquire methylation in the male germline, but also that they differ in their competence to maintain it postzygotically. In all the three

KI mouse lines, h1C1 was properly hypomethylated in oocytes but, contrary to the endogenous mouse locus, was methylated in a minority of sperm cells, indicating the inability of the human allele to properly establish DNA methylation in male germ cells (Fig. 8B). Conversely, the three h1C1 alleles showed a different capacity to maintain methylation after fertilization. While h1C1wt completely lost methylation on the paternal allele during development, h1C1Δ1.8 partially maintained it in one third of the animals, and h1C1Δ2.2 acquired mosaic methylation on both maternal and paternal alleles (Fig. 8B). The stronger CTCF binding to the h1C1wt and h1C1Δ1.8 alleles compared to h1C1Δ2.2 suggests that the number of CTSs is critical to control the level of h1C1 methylation during development, in the mouse context. However, we cannot exclude that other factors are involved in the control of *de novo* methylation and methylation maintenance of h1C1. Indeed, both the mouse and human IC1 harbor binding sites (one and three, respectively) (24) formed by single or multiple motifs recognized by the pluripotency factors OCT4 and SOX2 that have been demonstrated to cooperate with CTCF to maintain the unmethylated status of the maternal IC1

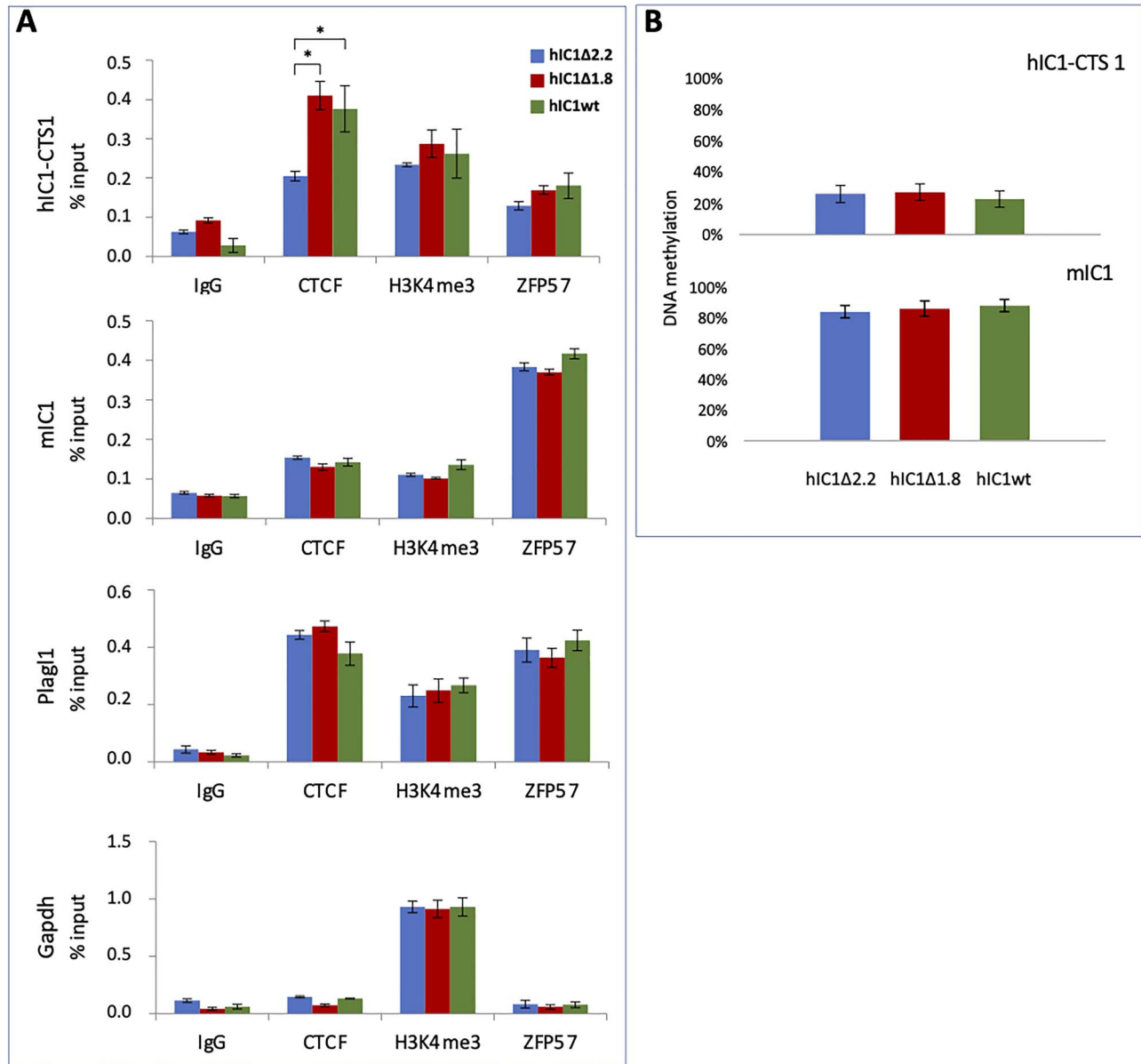


Figure 7. CTCF binding to the three hIC1 alleles in mouse ESCs. (A) ChIP analysis of CTCF, H3K4me3 and ZFP57 enrichment at CTS1 of the hIC1 transgenes and at the endogenous IC1 (mIC1), *Plag1* and *Gapdh* loci. The last two loci were analyzed as positive and negative controls, respectively. (B) Percent methylation at CTS1 of the hIC1 transgenes (hIC1-CTS1) and at the endogenous IC1 (mIC1), as measured by pyrosequencing. Bars represent the mean \pm SD.

(25). Several point mutations affecting one of the OCT4/SOX2 binding sites within the human maternal IC1 are associated with IC1 GOM and BWS phenotype (26). Also, a small deletion disrupting a binding site formed by a single SOX2 motif has been identified in a BWS case with IC1 GOM (26). Since the OCT4 binding site is lost on both hIC1 Δ 1.8 and hIC1 Δ 2.2 alleles and the SOX2 binding site is lost in hIC1 Δ 2.2 (15), it is possible that these factors in combination with CTCF influence the epigenetic status of the humanized IC1 alleles during mouse development.

In humans, the IC1 Δ 1.8 mutation has been associated with higher penetrance of imprinting defects, BWS phenotype and increased risk of developing Wilms tumors compared to IC1 Δ 2.2 (17) on maternal transmission, and proper methylation and imprinting and healthy phenotype on paternal transmission (17). This has led to the hypothesis that proper CTS spacing

rather than the number of CTSs is relevant for imprinting maintenance. Instead, this study demonstrates that, at least in the mouse context, the number of CTSs seems crucial to control hIC1 methylation and *H19/Igf2* imprinting, representing a further example of evolutionarily divergent imprinting mechanisms at the *H19/Igf2* locus.

Materials and Methods

Targeting of the mIC1 locus and generation of the KI mice

In order to generate the hIC1 Δ 1.8 mouse line, we carried out gene targeting by homologous recombination in E14 embryonic stem (ES) cells to replace the endogenous mIC1 with a plasmid containing the hIC1 Δ 1.8 allele and neomycin resistance cassette

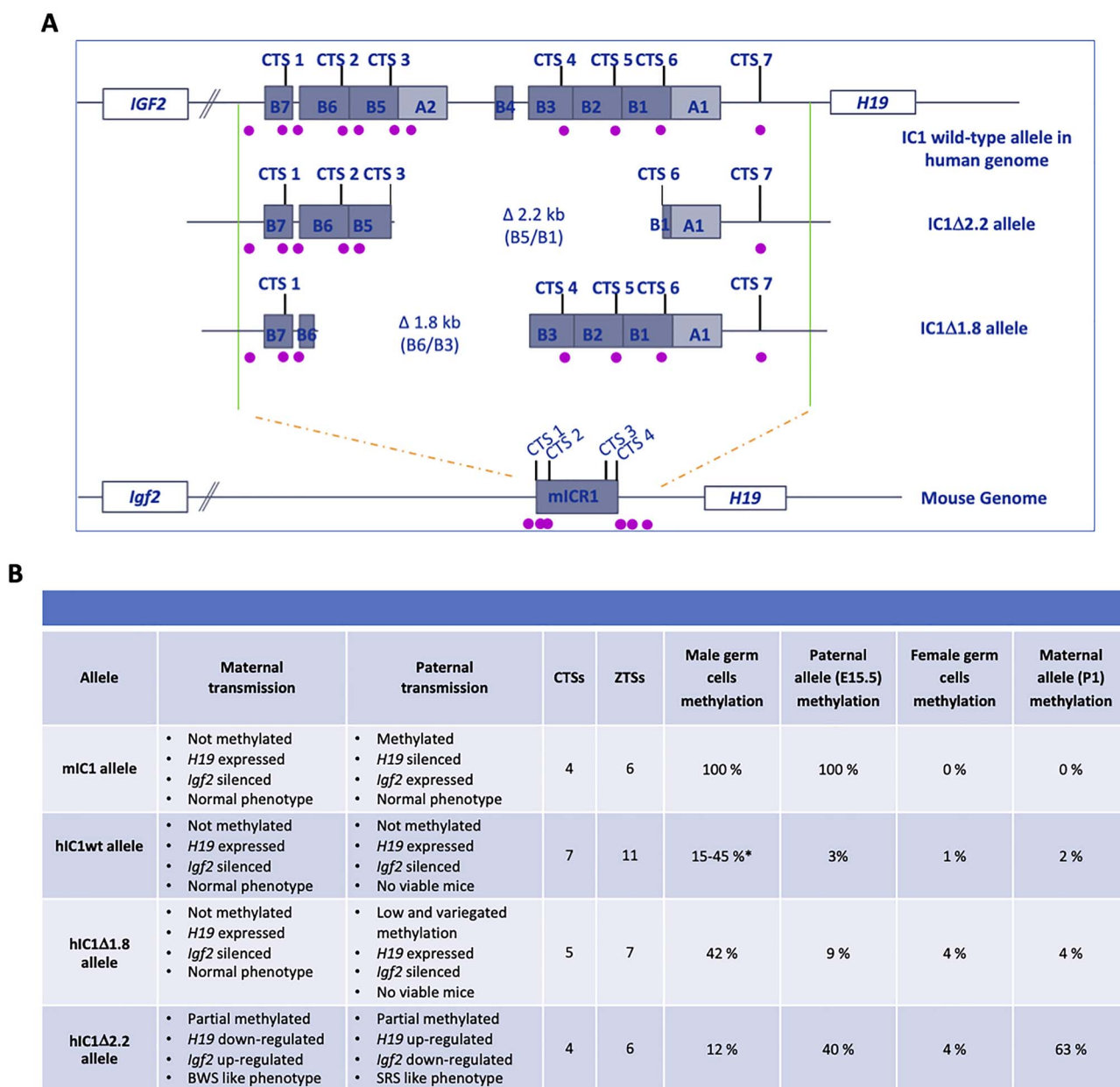


Figure 8. Summary of the characteristics and properties of the endogenous (miC1) and humanized (hiC1wt, hiC1Δ2.2 and hiC1Δ1.8) IC1 alleles. (A) Schematic representation showing the organization of the wild-type and mutant human and mouse IC1, with indication of A-type and B-type repeats, CTSs and ZTSs (purple dots). (B) Table summarizing the molecular and phenotypic characteristics of the human and mouse IC1 alleles. *The methylation levels of the hiC1wt mice derive from two different studies (20,23).

(NeoR; Fig. 1A). A *PciI*-*PciI* restriction fragment of 440 bp in length, containing the break-point of the 1.8 kb deletion found in a BWS family (13), was excised from the EΔ1.8 (B5/B2)pL vector (17), and subcloned into the wild type hiC1 region already cloned in the Δ3.8 kb-5' pre-targeting vector (27) by using the restriction enzyme *PciI*. The steps to obtain the targeting vector were performed as previously described (20,23). To confirm the correct targeting of ES clones, we performed Southern blot analysis of 5' and 3' arms, using two different probes (Fig. 1B). Injection into C57BL/6 (B6) blastocysts of the hiC1^{Δ1.8-neo} KI ES clones and generation of chimeras were obtained by Cogentech Facility S.c.a.r.l. (Milan, Italy). Chimeric mice were crossed to B6 mice. Germline transmission of the KI allele was detected in the agouti progeny by PCR-genotyping using primers flanking the deletion

break point (hDMDdelF2: 5'-GTTCCCGAGGGTTGTCAGAGATAG-3'; hDMDdelRev: 5'-CCCAGATGTGGCTCCCATGAATGTC-3'). The neoR cassette was excised by crossing heterozygous KI mice with pCX-NLS-Cre transgenic mice (28) on a B6 background. Excision was tested by PCR using primers flanking the neoR cassette (NeoEXL3: 5'-ACAGAATCGGTTGTGGCTGT-3' H19SeqR1: 5'-CCACAGAGTCAGCATCCAC-3') (Fig. 1C). KI mice were crossed with B6 mice and only the progeny carrying the KI and missing the Cre gene was used for further analysis. All animal experimentation was performed in accordance with the guidelines of the Animal Care and Use Committee of Campania University 'Luigi Vanvitelli' (Naples, Italy) and was authorized by the Italian Ministry of Health (Last two authorizations: 760/2016-PR and 178/2020-PR).

Molecular analyses

For extraction of nucleic acids, liver, kidneys and tongue were collected from the mice at birth (P1) and at 14 weeks of age. Total body (excluding the head) and placenta tissues were collected from conceptuses at 15.5 days post coitum (E15.5). Genomic DNA was isolated as previously described (23). Unfertilized oocytes were collected from four superovulated 8 week-old females and resuspended in 0.03% SDS, 10 mg glycogen, 10 mg proteinase K and 1× PBS to a final volume of 20 µl. The suspension was incubated at 37°C for 90 min followed by 15 min at 95°C and then used for DNA methylation analysis. Sperm cells were collected from two H19^{hiC1Δ1.8/+} males. Epididymis were separately immersed in PBS 1x (pH 7.6) and cut to let sperm cells flow out from the ducts. Cells were then filtered throughout cheesecloth to eliminate epididymal tissue fragments, centrifugated at 1500 × g for 30 min at 4°C, and incubated with a Somatic Cell Lysis Buffer (SCLB) [0.1% SDS, 0.5% Triton X-100 in DEPC-H₂O] on ice for 30 min to eliminate possible contaminant somatic cells. Sperm cells were centrifugated at 800 × g for 15 min at 4°C. The pellet was washed twice with PBS 1× and genomic DNA was isolated as previously reported (23). About 2 mg were used for DNA methylation analysis.

Total and allele-specific gene expression and DNA methylation analyses were performed as previously described (23). Primers and PCR conditions are reported in [Supplementary Material, Table S1](#). For the statistical analysis, data are reported as the mean ± standard error of the mean (SEM), unless otherwise indicated. The significance of the difference between two groups (KI, wild-type) was determined by two-tailed Student's t-test with two-sample unequal variance. The number of animals analyzed, and biological or technical replicates are indicated in the figure legends. Differences with P-values ≤ 0.05 were considered significant. Pearson correlation was applied to calculate the correlation coefficient (ρ) measuring the strength of the relationship between the following pairs of parameters: body weights and CTS1/CTS6 methylation and H19/Igf2 expression. The value of the correlation coefficient varies between +1 and -1. A value of ±1 indicates a perfect degree of association between the two variables. As the correlation coefficient value goes towards 0, the relationship between the two variables will be weaker. The direction of the relationship is indicated by the sign of the coefficient; a + sign indicates a positive relationship and a - sign indicates a negative relationship.

Chromatin Immunoprecipitation (ChIP) was performed as previously described (29). The following conditions were used: for CTCF, 7 µg of Diagenode C15410210 for 100 µg of chromatin in 600 µl of shearing buffer; for H3K4me3, 7 µg of Abcam ab8895 for 100 µg of chromatin in 600 µl of shearing buffer; and for ZFP57, 8 µg of Abcam ab45341 for 100 µg of chromatin in 600 µl of shearing buffer. The rabbit control IgG ChIP-grade antibody (5 µg of Abcam ab46540-1) was used as a control in the ChIP. Q-PCR assays of locus-specific ChIP were performed in triplicate on ABI PRISM 7500 using the default cycling conditions. Primers used for ChIP are listed in [Supplementary Material, Table S2](#). Each immunoprecipitated DNA was reported as percent of the input.

Supplementary Material

[Supplementary Material](#) are available at [HMGJ](#) online.

Acknowledgements

The authors thank the staff of the Animal facility of University of Campania 'Luigi Vanvitelli' for the valuable technical support.

Conflicts of Interest statement. The authors declare no conflict of interest.

Funding

AIRC-Associazione Italiana Ricerca sul Cancro (IG 2016 N.18671 and IG 2020 ID 24405 to A.R.); Telethon-Italia (GGP15131 to A.R.); 'Progetti per la ricerca oncologica della Regione Campania' Grant: I-Cure (to A.R. and F.C.), 'Progetti competitivi intraAteneo' Programma V:ALERE (VANviteLli pEr la RicERca) 2019—grant MIRIAM from Università degli Studi della Campania 'Luigi Vanvitelli' (to A.R., F.C. and A.S.), NIH grant (GM51279 to M.S.B.).

References

- Barlow, D.P. and Bartolomei, M.S. (2014) Genomic imprinting in mammals. *Cold Spring Harb. Perspect. Biol.*, **6**. doi: [10.1101/cshperspect.a018382](https://doi.org/10.1101/cshperspect.a018382).
- Monk, D., Mackay, D.J.G., Eggermann, T., Maher, E.R. and Riccio, A. (2019) Genomic imprinting disorders: lessons on how genome, epigenome and environment interact. *Nat. Rev. Genet.*, **20**, 235–248.
- Chang, S. and Bartolomei, M.S. (2020) Modeling human epigenetic disorders in mice: Beckwith-Wiedemann syndrome and Silver-Russell syndrome. *Dis. Model. Mech.*, **13**. doi: [10.1242/dmm.044123](https://doi.org/10.1242/dmm.044123).
- DeChiara, T.M., Efstratiadis, A. and Robertson, E.J. (1990) A growth-deficiency phenotype in heterozygous mice carrying an insulin-like growth factor II gene disrupted by targeting. *Nature*, **345**, 78–80.
- Gabory, A., Jammes, H. and Dandolo, L. (2010) The H19 locus: role of an imprinted non-coding RNA in growth and development. *BioEssays*, **32**, 473–480.
- Keniry, A., Oxley, D., Monnier, P., Kyba, M., Dandolo, L., Smits, G. and Reik, W. (2012) The H19 lincRNA is developmental reservoir of miR-675 that suppresses growth and Igf1r. *Nat. Cell Biol.*, **14**, 659–665.
- Qiu, X., Vu, T.H., Lu, Q., Ling, J.Q., Li, T., Hou, A., Wang, S.K., Chen, H.L., Hu, J.F. and Hoffman, A.R. (2008) A complex deoxyribonucleic acid looping configuration associated with the silencing of the maternal Igf2 allele. *Mol. Endocrinol.*, **22**, 1476–1488.
- Hark, A.T., Schoenherr, C.J., Katz, D.J., Ingram, R.S., Levorse, J.M. and Tilghman, S.M. (2000) CTCF mediates methylation-sensitive enhancer-blocking activity at the H19/Igf2 locus. *Nature*, **405**, 486–489.
- Bell, A.C. and Felsenfeld, G. (2000) Methylation of a CTCF-dependent boundary controls imprinted expression of the Igf2 gene. *Nature*, **405**, 482–485.
- Wakeling, E.L., Brioude, F., Lokulo-Sodipe, O., O'Connell, S.M., Salem, J., Blied, J., Canton, A.P., Chrzanoska, K.H., Davies, J.H., Dias, R.P. et al. (2017) Diagnosis and management of Silver-Russell syndrome: first international consensus statement. *Nat. Rev. Endocrinol.*, **13**, 105–124.
- Brioude, F., Kalish, J.M., Mussa, A., Foster, A.C., Blied, J., Ferrero, G.B., Boonen, S.E., Cole, T., Baker, R., Bertolotti, M.

- et al. (2018) Expert consensus document: clinical and molecular diagnosis, screening and management of Beckwith-Wiedemann syndrome: an international consensus statement. *Nat. Rev. Endocrinol.*, **14**, 229–249.
12. Anvar, Z., Acurzio, B., Roma, J., Cerrato, F. and Verde, G. (2019) Origins of DNA methylation defects in Wilms tumors. *Cancer Lett.*, **457**, 119–128.
 13. Sparago, A., Cerrato, F., Vernucci, M., Ferrero, G.B., Silengo, M.C. and Riccio, A. (2004) Microdeletions in the human H19 DMR result in loss of IGF2 imprinting and Beckwith-Wiedemann syndrome. *Nat. Genet.*, **36**, 958–960.
 14. Sparago, A., Russo, S., Cerrato, F., Ferraiuolo, S., Castorina, P., Selicorni, A., Schwienbacher, C., Negrini, M., Ferrero, G.B., Silengo, M.C. et al. (2007) Mechanisms causing imprinting defects in familial Beckwith-Wiedemann syndrome with Wilms' tumour. *Hum. Mol. Genet.*, **16**, 254–264.
 15. Sparago, A., Cerrato, F. and Riccio, A. (2018) Is ZFP57 binding to. *Clin. Epigenetics*, **10**, 23. doi: [10.1186/s13148-018-0454-7](https://doi.org/10.1186/s13148-018-0454-7).
 16. Cerrato, F., Sparago, A., Di Matteo, I., Zou, X., Dean, W., Sasaki, H., Smith, P., Genesio, R., Bruggemann, M., Reik, W. et al. (2005) The two-domain hypothesis in Beckwith-Wiedemann syndrome: autonomous imprinting of the telomeric domain of the distal chromosome 7 cluster. *Hum. Mol. Genet.*, **14**, 503–511.
 17. Beygo, J., Citro, V., Sparago, A., De Crescenzo, A., Cerrato, F., Heitmann, M., Rademacher, K., Guala, A., Enklaar, T., Anichini, C. et al. (2013) The molecular function and clinical phenotype of partial deletions of the IGF2/H19 imprinting control region depends on the spatial arrangement of the remaining CTCF-binding sites. *Hum. Mol. Genet.*, **22**, 544–557.
 18. Abi Habib, W., Brioude, F., Azzi, S., Salem, J., Das Neves, C., Personnier, C., Chantot-Bastaraud, S., Keren, B., Le Bouc, Y., Harbison, M.D. et al. (2017) 11p15 ICR1 partial deletions associated with IGF2/H19 DMR hypomethylation and Silver-Russell syndrome. *Hum. Mutat.*, **38**, 105–111.
 19. Kraft, F., Wesseler, K., Begemann, M., Kurth, I., Elbracht, M. and Eggermann, T. (2019) Novel familial distal imprinting Centre 1 (11p15.5) deletion provides further insights in imprinting regulation. *Clin. Epigenetics*, **11**, 30. doi: [10.1186/s13148-019-0629-x](https://doi.org/10.1186/s13148-019-0629-x).
 20. Hur, S.K., Freschi, A., Ideraabdullah, F., Thorvaldsen, J.L., Luense, L.J., Weller, A.H., Berger, S.L., Cerrato, F., Riccio, A. and Bartolomei, M.S. (2016) Humanized H19/Igf2 locus reveals diverged imprinting mechanism between mouse and human and reflects Silver-Russell syndrome phenotypes. *Proc. Natl. Acad. Sci. USA.*, **113**, 10938–10943.
 21. Cerrato, F., Sparago, A., Verde, G., De Crescenzo, A., Citro, V., Cubellis, M.V., Rinaldi, M.M., Boccutto, L., Neri, G., Magnani, C. et al. (2008) Different mechanisms cause imprinting defects at the IGF2/H19 locus in Beckwith-Wiedemann syndrome and Wilms' tumour. *Hum. Mol. Genet.*, **17**, 1427–1435.
 22. Duffy, K.A., Cielo, C.M., Cohen, J.L., Gonzalez-Gandolfi, C.X., Griff, J.R., Hathaway, E.R., Kupa, J., Taylor, J.A., Wang, K.H., Ganguly, A. et al. (2019) Characterization of the Beckwith-Wiedemann spectrum: diagnosis and management. *Am. J. Med. Genet. C Semin. Med. Genet.*, **181**, 693–708.
 23. Freschi, A., Hur, S.K., Valente, F.M., Ideraabdullah, F.Y., Sparago, A., Gentile, M.T., Oneglia, A., Di Nucci, D., Colucci-D'Amato, L., Thorvaldsen, J.L. et al. (2018) Tissue-specific and mosaic imprinting defects underlie opposite congenital growth disorders in mice. *PLoS Genet.*, **14**, e1007243. doi: [10.1371/journal.pgen.1007243](https://doi.org/10.1371/journal.pgen.1007243).
 24. Shmela, M.E. and Gicquel, C.F. (2013) Human diseases versus mouse models: insights into the regulation of genomic imprinting at the human 11p15/mouse distal chromosome 7 region. *J. Med. Genet.*, **50**, 11–20.
 25. Zimmerman, D.L., Boddy, C.S. and Schoenherr, C.S. (2013) Oct4/Sox2 binding sites contribute to maintaining hypomethylation of the maternal igf2/h19 imprinting control region. *PLoS One*, **8**, e81962.
 26. Abi Habib, W., Azzi, S., Brioude, F., Steunou, V., Thibaud, N., Das Neves, C., Le Jule, M., Chantot-Bastaraud, S., Keren, B., Lyonnet, S. et al. (2014) Extensive investigation of the IGF2/H19 imprinting control region reveals novel OCT4/SOX2 binding site defects associated with specific methylation patterns in Beckwith-Wiedemann syndrome. *Hum. Mol. Genet.*, **23**, 5763–5773.
 27. Thorvaldsen, J.L., Mann, M.R., Nwoko, O., Duran, K.L. and Bartolomei, M.S. (2002) Analysis of sequence upstream of the endogenous H19 gene reveals elements both essential and dispensable for imprinting. *Mol. Cell. Biol.*, **22**, 2450–2462.
 28. Nagy, A. (2000) Cre recombinase: the universal reagent for genome tailoring. *Genesis*, **26**, 99–109.
 29. Anvar, Z., Cammisa, M., Riso, V., Baglivo, I., Kukreja, H., Sparago, A., Girardot, M., Lad, S., De Feis, I., Cerrato, F. et al. (2016) ZFP57 recognizes multiple and closely spaced sequence motif variants to maintain repressive epigenetic marks in mouse embryonic stem cells. *Nucleic Acids Res.*, **44**, 1118–1132.